American Mineralogist, Volume 79, pages 996–1002, 1994

Fetiasite (Fe^{2+}, Fe^{3+}, Ti)$_3O_2$ [As_2O_5], a new arsenite mineral: Its description and structure determination

Stefan Graeser
Natural History Museum, CH-4001 Basel, Switzerland
and Mineralogical Institute, University of Basel, CH-4056 Basel, Switzerland

Hans Schwander
Mineralogical Institute, University of Basel, CH-4056 Basel, Switzerland

Francesco Demartin
Istituto di Chimica Strutturistica Inorganica, Università degli Studi, via Venezian 21, I-20133 Milan, Italy

Carlo M. Gramaccioli
Dipartimento di Scienze della Terra, Università degli Studi, via Botticelli 23, I-20133 Milan, Italy

Tullio Pilati
CNR, Centro per lo Studio delle Relazioni tra Struttura e Reattività Chimica, via Golgi 19, I-20133 Milan, Italy

Eric Reusser
Institute for Mineralogy and Petrography, ETH Zurich, CH-8092 Zurich, Switzerland

Abstract

Fetiasite, (Fe^{2+}, Fe^{3+}, Ti^{4+})$_3O_2As_2^{3+}O_5$, is a new mineral found at Pizzo Cervandone, Italy, and Binntal, Switzerland, in the Central Alps. Fetiasite is monoclinic, $P2_1/m$, $Z = 2$, $a = 10.614(2)$, $b = 3.252(1)$, $c = 8.945(1)$ Å, $\beta = 108.95(2)°$; $V = 291.9(2)$ Å^3. The strongest powder-diffraction lines [d_{obs} (Å), (hkl), I/I_0] are as follows: 2.749, (210, $\bar{2}$11),100; 2.814, (202,301),94; 2.391,(110),85; 2.985,($\bar{1}$03),67; 1.779,($\bar{5}$04,$\bar{5}$11),48; 1.709,(510,$\bar{6}$03),35; 1.754,(204,$\bar{6}$01),32; 3.526,(102),31. Fetiasite is brown to black, has a metallic to semimetallic luster, and shows perfect cleavage on {100}. Microhardness VHN_{50} = 440–490 kg/mm^2 corresponding to a Mohs hardness of ≈5; $D_{obs} = 4.6$, $D_{calc} = 4.74$–4.80 g/cm^3. In polished section, the mineral appears creamy white; anisotropy is visible along the grain boundaries. Reflectance values (in air) are 15.4–16.0% (470 nm), 15.3–15.8% (546 nm), 14.8–15.2% (589 nm), 14.2–15.0% (650 nm).

Fetiasite and other associated arsenic minerals (e.g., asbecasite, cafarsite, cervandonite) are products of As-bearing solutions remobilized from pre-Alpine ore concentrations (tennantite, chalcopyrite) by Alpine metamorphism.

The crystal structure was solved and refined to $r = 0.029$ for 1168 observed reflections (Pizzo Cervandone) and to $r = 0.023$ for 1200 observed reflections (Binntal). The structure contains two As_2O_5 groups, with the As^{3+} cations in trigonal pyramidal coordination, and three nonequivalent octahedral sites, two essentially occupied by Fe and one statistically occupied by Fe and Ti. The octahedra are joined together by sharing edges and corners to form a framework, characterized by the presence of channels running along [010], in which the As atoms are situated.

Introduction

The new mineral fetiasite was first found by the Italian mineral collector Claudio Albertini in 1986 in the mountain region of Pizzo Cervandone (3155 m above sea level) that forms the border between Italy (Alpe Devero) and Switzerland (Binntal, Canton Valais). This region has become famous since the 1960s for a remarkable number of rare and new minerals, mainly arsenites and arsenates (e.g., asbecasite, cafarsite: Graeser, 1966; Graeser and Roggiani, 1976; gasparite: Graeser and Schwander, 1987; cervandonite: Armbruster et al., 1988). The first specimen of fetiasite was found at about 3000 m above sea level at the eastern slope of Pizzo Cervandone in Italy. Shortly thereafter, the same mineral was detected by Swiss collectors (A. Skrapits, A. Gorsatt, R. Lüssi) about 4 km to the north in two mineral fissures at Gorb in Binntal (formerly well known for the occurrence of spectacular anatase crystals). Material from this locality, though completely different in size and morphology, was essentially identical in other features to that from the Italian occurrence. Therefore, it seems reasonable to give the status of type locality to both occurrences.

0003–004X/94/0910–0996$02.00

TABLE 1. Physical and optical data of fetiasite

Color: brown to black	Luster: metallic to semimetallic
Cleavage: {100} perfect	Fracture: uneven to conchoidal
Hardness: VHN_{50} = 438 kg/mm² (430–447)	} on two crystals
VHN_{50} = 490 kg/mm² (487–494)	} on two crystals
Mohs = ≈5 (according to VHN)	

D_{pycn} = 4.6(1) g/cm³ → low because of alteration (locality C)
D_{calc} = 4.74 g/cm³ (locality A); D_{calc} = 4.80 g/cm³ (locality B)

Observations in reflected light (Leitz MPV compact)

	In air	In oil (N = 1.515)
Color	creamy white	white, with weak brown tint
Internal refl.	none observed	none observed
Anisotropy	visible along grain boundaries	clearly visible
Bireflectance	not visible	very weak along grain boundaries

Reflectance values for two isolated crystals at COM wavelengths (SiC standard, minimum and maximum values)

470 nm: 15.4–16.0%	4.17–5.12%
546 nm: 15.3–15.8%	3.69–4.68%
589 nm: 14.8–15.2%	3.70–4.53%
650 nm: 14.2–15.0%	3.79–4.26%

Fig. 1. Fetiasite aggregates (2 mm across) from locality A. Photograph by W. Gabriel.

The name fetiasite was derived from the mineral's chemical composition Fe-Ti-As oxide. The type material is preserved at the Department of Mineralogy, Natural History Museum, Basel, and at the Mineralogical Institute, University of Basel. The mineral and the mineral name have been accepted by the Commission on New Minerals and Mineral Names, IMA.

GEOLOGICAL SITUATION

The whole mountain range between Alpe Devero and Binntal is built up partly by serpentinites and mainly by gneisses belonging to the Monte Leone nappe, one of the lower units of the Pennine Simplon nappes. The host rocks at the two occurrences are gneisses of variable mineral composition that were influenced by Alpine metamorphism in upper greenschist to lower amphibolite facies; the accompanying Mesozoic calcareous metasediments (Bündnerschiefer) contain abundant kyanite of Alpine origin. The whole region is characterized by a remarkable positive anomaly of the element As. This is manifested by the occurrence of a large number of very special arsenic oxide minerals (arsenites and arsenates), a number of which have been determined as new minerals within the last 25 yr. Presumably, this As anomaly has been caused by a remobilization process during Alpine metamorphism of primary Cu- and As-bearing sulfide ores (tennantite) of Hercynian age, which, in a later state, was responsible for the formation of arsenic sulphosalts in the Triassic dolomite at the famous locality Lengenbach, Binntal (Graeser, 1966; Graeser and Roggiani, 1976). It is not yet clear if there is an age difference between the formation of the arsenites, which were probably formed at an earlier stage, and the arsenates, which are probably the product of subsequent oxidation under atmospheric conditions.

The three occurrences (subsequently designated as A, B, and C) of fetiasite are clearly distinguishable by the morphology of the respective crystals. That fetiasite from the three localities is chemically and structurally identical, whereas the host rocks are different, suggests deposition by migrating As-bearing solutions.

Locality A is at Pizzo Cervandone, Italy, about 3000 m above sea level. The first small fetiasite aggregates (up to 2 mm) were found in an Alpine mineral fissure in a light-colored, feldspar-rich, two-mica gneiss of presumably orthogneiss character. The sample contained abundant chlorite (ripidolite), small colorless quartz crystals, and some anatase.

Localities B and C are at Binntal, Switzerland. Fetiasite was detected here in two fissures in dark crystalline rocks ranging from biotite-rich gneisses to mica schists. This is the region that, under the name Lercheltini-Zone, had a worldwide reputation for its spectacular anatase crystals early in this century. The fetiasite crystals from here were collected in the old abandoned clefts that had been mined for anatase about 100 yr ago; surprisingly, these professional mineral collectors ("Strahler") overlooked the new mineral for many years, as well as asbecasite, cafarsite, and cervandonite. The fissures containing fetiasite and these other As minerals are located at about 2000 m above sea level.

PHYSICAL AND OPTICAL PROPERTIES

All fetiasite crystals are covered by a thin brown-red alteration layer that renders the mineral difficult to recognize. Beneath this alteration, fetiasite exhibits the physical properties given in Table 1.

Although the chemical and structural data are identical, the crystal morphology is remarkably different at the three localities: At locality A, only a single hand specimen exists; it consisted of several minute tabular crystals about 0.2 mm in diameter, forming globular aggregates of pinecone shape, rarely exceeding 2 mm in diameter (Fig. 1). On splitting up these aggregates to select single crystals, a perfect cleavage was always observed, on {100}, according to single-crystal X-ray study. At locality B, fe-

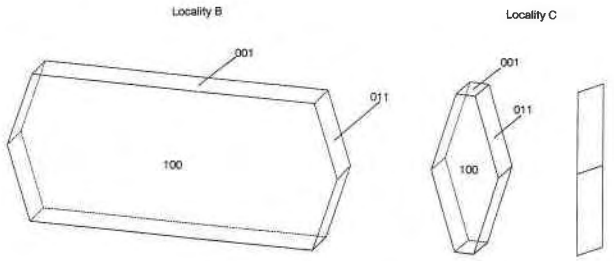

Fig. 2. Idealized crystal drawings (Shape) of fetiasite from locality B and locality C; crystal at right is viewed along **b**.

tiasite occurs as radial aggregates (up to 40 mm across) of shingle-shaped crystals of 20 mm maximum length. By analogy with the crystals from locality C (measured by an optical goniometer), fetiasite at locality B is elongated along the **b** axis, with the following forms present: *a* {100}, *c* {001}, *m* {011}. The perfect cleavage on {100} is easily recognizable (see Fig. 2a). At locality C, about 5 m above locality B, characteristic isolated fetiasite crystals reach 1 cm in length and have a peculiar boat-like shape. It was possible to measure a fragment of one of these crystals with an optical goniometer (see Table 2). In agreement with the single-crystal X-ray study, the following forms were identified: *a* {100}, *c* {001}, *m* {011}. In contrast to the crystals of the other localities mentioned above, fetiasite from locality C is slightly elongated along the **c** axis and is platy on {100} (see Fig. 2b). These crystals, like the corresponding ones from localities A and B, are superficially altered to an X-ray amorphous powder of brown-red color.

Chemical composition

Preliminary qualitative analyses of the mineral were obtained with SEM-EDS techniques (Cambridge Stereoscan Mark 2A). The EDS analyses revealed the presence of Fe, Ti, and As only, with no substantial quantities of other elements. Comparison of the IR spectrum (Perkin Elmer 883) of fetiasite with the spectra of magnussonite (Långban, Sweden) and mimetite (Tsumeb mine, Namibia) showed fetiasite to be an arsenite mineral, with As as As^{3+} (see Fig. 3).

The chemical analyses were carried out by means of an ARL electron microprobe using the following standards: quartz (Si), corundum (Al), rutile (Ti), FeOOH and fayalite (Fe), MnOOH and spessartine (Mn), $AlAsO_4$ (As), wollastonite (Ca), and NaF and albite (Na). The results

Table 2. Measurements from the optical goniometer

Form	ϕ_{obs} (°)	ρ_{obs} (°)	ϕ_{calc} (°)	ρ_{calc} (°)
001	90	19.1	90	19.1
100	90	90	90	90
011	7	70	7.2	70.03

Note: measurements were made on fetiasite, locality C; *a*:1:*c* = ∞:1:2.73, β = 109.1° (from goniometry); *a*:1:*c* = 3.26:1:2.75, β = 108.95° (X-ray study).

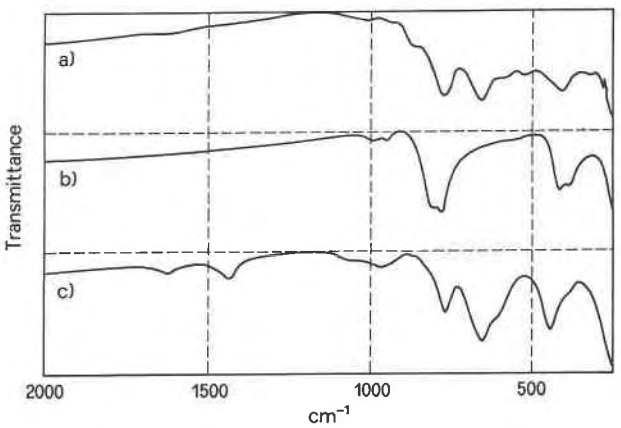

Fig. 3. Infrared spectra of arsenite and arsenate minerals (IR-Laboratorium, MPI, Basel). (a) (IR 049) fetiasite, Cervandone, Italy; (b) (IR 142) mimetite, Tsumeb mine, Namibia; (c) (IR 298) magnussonite, Långban, Sweden.

of the crystal structure determination (see the next section) showed Fe to be present as Fe^{2+} and Fe^{3+}, with a Fe^{2+}/Fe^{3+} ratio of 1.5. The final electron microprobe results are presented in Table 3. Fetiasite crystals from the two localities, Pizzo Cervandone, Italy (A), and Binntal, Switzerland (B), are virtually identical; there is good agreement between the microprobe data and the results of the structure determination.

X-ray diffraction study

Single-crystal photographs (Weissenberg and precession techniques) showed monoclinic symmetry, with conditions for nonextinction ($0k0$: $k = 2n$) consistent with the possible space groups $P2_1/m$ or $P2_1$; the subsequent structure determination showed $P2_1/m$ to be correct. This is in agreement with the evident centrosymmetric crystal habit of the idiomorphic fetiasite crystals found later (locality C). The powder diffraction pattern is reported in Table 4, and the unit-cell data are reported in Table 5.

The crystal from locality A used for structure determination was a cleavage plate with largest dimensions 0.10 × 0.09 mm; the crystal from locality B was 0.08 × 0.07 × 0.10 mm. Both crystals were mounted on an Enraf-Nonius CAD-4 diffractometer, and 25 intense reflections having a θ value in the range 12.6–20.1° were centered using graphite-monochromated Mo$K\alpha$ radiation (λ = 0.71073 Å). Least-squares refinement of their setting angles resulted in the unit-cell parameters reported in Table 5, together with an orientation matrix relating the crystal axes to the diffractometer axes. A total of 2940 diffracted intensities for sample A and 2925 for sample B were collected at room temperature with variable scan speed (the maximum scan time for each reflection was 90 s), with $-17 \leq h < 17$, $0 \leq k \leq 5$, and $-15 \leq l \leq 15$, to a maximum 2θ angle of 70°. An ω scan was used in the collection of the intensities of sample A, whereas a $\theta/2\theta$ scan was used for sample B. The diffracted intensities were corrected for Lorentz, polarization, and background

TABLE 3. Chemical composition of fetiasite

	Locality A		Locality B	
	I	II	III	IV
FeO	23.12	23.69	24.23	23.84
Fe_2O_3*	17.13	17.58	17.93	17.64
MnO	1.25	1.27	0.89	0.84
TiO_2	10.09	10.37	11.17	10.95
As_2O_3	46.95	47.09	46.76	46.73
Total	98.54	100.00	100.98	100.00
Fe^{2+}	1.38		1.40	
Mn	0.08		0.05	
Fe^{3+}	0.92		0.93	
Ti	0.54		0.58	
Total	2.92		2.96	
As	2.0		2.0	
O	7.0		7.0	

Note: I = mean of seven individual analyses of fetiasite (locality A); II = $(Fe^{2+}_{1.38}Fe^{3+}_{0.92}Ti_{0.54}Mn_{0.08})_{\Sigma=2.92}[O_2|As_2O_5]$; III = mean of ten individual analyses of fetiasite (locality B); IV = $(Fe^{2+}_{1.40}Fe^{3+}_{0.93}Ti_{0.58}Mn_{0.05})_{\Sigma=2.96}[O_2|As_2O_5]$.

* The ratio $Fe^{2+}/Fe^{3+} = 1.5$ is from structure determination.

TABLE 4. X-ray powder diffraction data for fetiasite

	Locality A*			Locality B**		Locality C†	
hkl	d_{calc}	d_{obs}	I/I_0	d_{calc}	d_{obs}	d_{calc}	d_{obs}
001	8.493	8.5	12	8.465	8.43	8.45	8.41
$\bar{1}02$	4.472	4.48	21	4.453	4.45	4.442	4.441
002	4.246	4.25	10	4.233	—	4.223	4.220
$\bar{3}01$	3.533	3.526	31	3.529	3.528	3.522	3.525
102	3.518			3.512		3.506	
300	3.346	3.340	15	3.346	3.344	3.340	3.342
$\bar{3}02$	3.184	3.183	12	3.175	3.174	3.168	3.171
110	3.104	3.107	21	3.104	3.088	3.086	3.085
$\bar{1}03$	2.993	2.985	67	2.981	2.981	2.974	2.976
202	2.818	2.811	94	2.816	2.813	2.811	2.813
301	2.814			2.814		2.816	
$\bar{2}11$	2.752	2.749	100	2.750	2.740	2.737	2.737
210	2.736			2.736		2.723	
$\bar{1}12$	2.637	2.636	15	2.633	—	2.622	—
$\bar{3}03$	2.627			2.617		2.617	
$\bar{4}02$	2.559	2.563	27	2.553	2.554	2.548	2.548
$\bar{2}12$	2.514	2.510	25	2.510	—	2.499	2.499
400	2.509			2.509		2.505	
112	2.393	2.391	85	2.391	2.383	2.381	2.381
$\bar{1}14$	1.842	1.836	13	1.837	1.832	1.830	1.833
411	1.834			1.834		1.829	
$\bar{5}04$	1.779	1.779	48	1.773	1.771	1.768	1.769
$\bar{5}11$	1.775			1.774		1.769	
204	1.759	1.754	32	1.756	1.755	1.753	1.754
$\bar{6}01$	1.754			1.753		1.750	
510	1.710	1.709	35	1.710	1.708	1.705	1.705
$\bar{6}03$	1.706			1.702		1.699	
020	1.632	1.629	20	1.632	1.621	1.622	1.622
313	1.628			1.627		1.622	
502	1.621			1.621		1.618	
220	1.552	1.549	20	1.552	1.541	1.543	1.543
214	1.549			1.547		1.542	
601	1.548			1.548		1.546	
		1.459	32				1.455
		1.431	27				1.423
		1.412	16				1.404
a =	10.625(4) Å			10.615(3) Å		10.595(3) Å	
b =	3.264(2) Å			3.264(1) Å		3.244(1) Å	
c =	8.990(6) Å			8.952(3) Å		8.931(2) Å	
β =	109.15(4)°			108.98(2)°		108.95(5)°	
$a:1:c$ =	3.255:1:2.754			3.252:1:2.743		3.266:1:2.753	

Note: lattice parameters were refined from powder diagrams.

* Debye-Scherrer camera, 114.6 mm, Fe$K\alpha$.

** Guinier-IV camera, Fe$K\alpha_1$.

† Guinier-Hägg camera, Cu$K\alpha_1$.

effects. An empirical absorption correction was applied according to the procedure already described in Demartin et al. (1992); the minimum transmission factor is 0.42 and 0.63 for A and B, respectively. A total of 1470 independent reflections for A ($R_{av.}$ = 2.4%) and 1462 for B ($R_{av.}$ = 1.7%) were obtained, and only those with $I > 2\sigma_I$ were considered for the structure solution and refinement.

Scattering factors for neutral atoms, including anomalous dispersion corrections, were taken from Cromer and Waber (1974) and Cromer (1974), respectively. The structure was solved by direct methods using Multan (Germain et al., 1971) and refined by full-matrix least squares, minimizing the function $\Sigma w(F_o - k|F_c|)^2$. Weights assigned to individual observations were $1/\sigma^2(F_o)$, where $\sigma(F_o) = [\sigma_I^2 + (kI)^2]^{1/2}/2F_oLp$, σ_I^2 is the standard deviation for each reflection as derived from counting statistics, k (= 0.04) is a coefficient for improving the goodness of fit, and Lp is the Lorentz-polarization factor. Anisotropic displacement parameters were assigned to all the atoms. The refined extinction coefficients were 3.03×10^{-7} for A and 1.35×10^{-6} for B. The final R and R_w indices were 0.029 and 0.033 for 1168 reflections (sample A) and 0.023 and 0.030 for 1200 reflections (sample B), respectively. The maximum residual in the final difference-Fourier synthesis was 1.7 and 1.2 e/Å^3 for A and B, respectively. The fractional atomic coordinates and their estimated standard deviations are reported in Table 6. The anisotropic displacement parameters are reported in Table 7. Selected interatomic distances and angles are reported in Table 8. Observed and calculated structure factor amplitudes for samples A and B are reported in Tables 9A and 9B,[1] respectively.

[1] A copy of Table 9A and 9B may be ordered as Document AM-94-564 from the Business Office, Mineralogical Society of America, 1130 Seventeenth Street NW, Suite 330, Washington, DC 20036, U.S.A. Please remit $5.00 in advance for the microfiche.

DESCRIPTION OF THE STRUCTURE

The structure (Fig. 4) can be considered as belonging to the so-called "3-Å fiber axis wallpaper structures" (Moore and Araki, 1974; Konnert et al., 1976). It is characterized by three independent sites occupied by Fe and Ti atoms in octahedral coordination. The octahedra are joined together by sharing edges and corners to form a three-dimensional framework with channels extending along [010]. In these channels, As atoms are bound with trigonal pyramidal coordination to adjacent O atoms.

The As atoms are aligned along [010] at intervals corresponding to the value of the unit-cell parameter b, so that a sequence of atomic coordinates, $x,-¾,z$; $x,¼,z$; $x,¾,z$, etc., is observed. Each As atom is bound to two O atoms lying in the same plane normal to **b** (i.e., O5 and O6 for As1 and O1 and O2 for As2) and to a bridging O atom (i.e., O8 connecting two As1 atoms and O7 connecting two As2 atoms, respectively).

TABLE 5. Unit-cell data for fetiasite, $(Fe^{2+},Fe^{3+},Ti)_3O_2[As_2O_5]$

	Cervandone (A)	Binntal (B)	Binntal (C)
a (Å)	10.614(2)*	10.616(1)*	10.595(3)**
b (Å)	3.252(1)	3.242(1)	3.244(1)
c (Å)	8.945(1)	8.932(1)	8.931(2)
β (°)	108.95(2)	108.89(2)	108.95(5)
V (Å^3)	291.9(2)	290.9(2)	290.3(1)
Space group	$P2_1/m$	$P2_1/m$	$P2_1/m$
$Z = 2$			

* Single-crystal data.
** Refined from powder data (Guinier-Hägg).

TABLE 6. Fractional atomic coordinates and displacement parameters

Atom	Mult	x	y	z	B_{eq} (Å^2)
As1	0.50	0.40970(4)	¼	0.66474(5)	0.717(7)
		0.41010(3)	¼	0.66453(4)	0.792(5)
As2	0.50	0.24978(4)	¼	0.24797(5)	0.782(7)
		0.24954(3)	¼	0.24816(4)	0.831(5)
Fe1	0.50	0.04922(6)	¼	0.86648(7)	0.89(1)
		0.04912(5)	¼	0.86648(6)	0.902(8)
Fe2	0.50	0.64241(6)	¼	0.02199(7)	0.67(1)
		0.64280(4)	¼	0.02237(5)	0.719(7)
(Fe,Ti)	0.53*	0.88301(9)	¼	0.39371(9)	1.24(1)
	0.55*	0.88267(6)	¼	0.39356(7)	1.26(1)
O1	0.50	0.0815(3)	¼	0.1156(4)	1.41(7)
		0.0816(3)	¼	0.1159(3)	1.41(5)
O2	0.50	0.3292(4)	¼	0.1035(4)	1.50(7)
		0.3287(3)	¼	0.1036(3)	1.49(5)
O3	0.50	0.8322(3)	¼	0.1581(4)	1.09(6)
		0.8324(2)	¼	0.1586(3)	1.02(4)
O4	0.50	0.9930(3)	¼	0.6193(4)	1.76(8)
		0.9928(3)	¼	0.6192(3)	1.67(5)
O5	0.50	0.4332(3)	¼	0.8726(4)	1.26(6)
		0.4335(2)	¼	0.8722(3)	1.20(5)
O6	0.50	0.2348(4)	¼	0.5993(5)	3.2(1)
		0.2347(3)	¼	0.5990(3)	2.69(8)
O7	0.25	0.7279(7)	¼	0.6769(8)	1.4(1)
		0.7275(5)	¼	0.6763(6)	1.31(9)
O8	0.25	0.5520(9)	¼	0.3827(9)	2.1(2)
		0.5518(6)	¼	0.3834(7)	1.9(1)

Note: estimated standard deviations are in parentheses. First rows: sample A; second rows: sample B. Isotropic equivalent displacement parameter (B_{eq}) defined as $\frac{4}{3}(a^2B_{11} + b^2B_{22} + c^2B_{33} + ac(\cos\beta)B_{33})$.
* Refined as Ti.

Since the occupation factor for both O7 and O8 is 0.5, we clearly have a case of statistical disorder between empty and occupied sites, thereby excluding the presence of an infinite polyarsenate chain. This disorder is confirmed by other details; for instance, full occupancy of O7 and O8 would result in an O-O distance of 2.687(12) Å. However, such a short distance would be compatible only with the existence of a strong H bond, in this case contradicted by the absence of frequencies due to OH stretching in the infrared spectrum and of residual peaks in the expected position in the final difference-Fourier synthesis. The only way of avoiding this short distance is by short-range ordering of atoms and vacancies, leading to the average occupation of 0.5 that we have observed.

As this model of disorder involving the O atoms bound to the As atoms implies a strong correlation along the same channel, there must be a lack of correlation among different channels; otherwise, the b parameter would be a multiple of the value reported here. However, no additional reflections have been recorded, even from overexposed films in Weissenberg or precession cameras.

For the reasons discussed above, the mineral is clearly an arsenite, with two AsO_3^{3-} groups sharing a corner, forming an $As_2O_5^{4-}$ dimeric group. The geometry matches the corresponding data reported by Hawthorne (1985) for a series of natural arsenites.

DISCUSSION

The chemical formula for fetiasite can be written as $Me_3As_2O_7$, or $Me_3O_2[As_2O_5]$ if the presence of $As_2O_5^{4-}$ groups is emphasized. Unlike the AsO_4^{3-} ion, AsO_3^{3-} even in nature easily forms polymeric clusters. For instance, a tetrameric $As_4O_8^{4-}$ group occurs in stenhuggarite, $CaFeSbAs_2O_7$ (Coda et al., 1977), whereas indefinite arsenite chains can be observed in trippkeite, $CuAs_2O_4$ (Zemann, 1951; Pertlik, 1975), and in the corresponding (not isostructural) zinc compound leiteite, $ZnAs_2O_4$ (Ghose et al., 1987). Similar to fetiasite, dimeric $As_2O_5^{4-}$ groups also occur in paulmooreite, $Pb_2[As_2O_5]$ (Araki et al., 1980), and in schneiderhöhnite, $Fe^{2+}Fe_3^{3+}As_5O_{13}$ (Hawthorne, 1985). In these minerals, the average As-O distances in the dimeric groups are 1.778(4) and 1.784(2) Å, respectively, which are significantly longer than the corresponding average value in fetiasite [1.767(1) Å].

In fetiasite, Me essentially corresponds to a mixture of Fe and Ti, and, for that reason, the formula could be alternatively written as $(Fe,Ti)_3O_2[As_2O_5]$. Since these two metals are present in three crystallographic sites, the composition of each of these sites is not necessarily the same as for the others, even in the same sample. Refinement of the occupation parameter of these sites confirmed by the value of the relative bond-length averages (see below) indicates the virtual absence of Ti in the sites indicated as Fe1 and Fe2.

A complication arises from considering the oxidation state of Fe and Ti in the mineral. Since, as we have seen, As is in the +3 state, a total of eight formal electron charges should be assigned to Fe, Ti, and Mn in the three sites. If Ti is all in the +4 state and Mn is in the +2 state, this would correspond to a total of $0.55 \times 4 = 2.20$ formal charges for the sample from Cervandone, and the remaining $8 - 2.20 - 0.14 = 5.66$ formal charges should be attributed to the Fe atoms, leading to a fractional average oxidation state of $5.66/2.30 = 2.46$. This value implies the presence of both Fe^{2+} and Fe^{3+}; similar cases are encountered in a number of complex oxides of transition elements, both natural and artificial. In the same way, an average oxidation state of 2.39 can be deduced for the sample from Binntal. From these considerations, a Fe^{2+}-Fe^{3+} ratio of about 1.5 can be assumed in our specimens.

This estimate for the average oxidation state for Fe may change noticeably if Ti is considered to be in the +3

TABLE 7. Anisotropic displacement factors

Atom	U_{11}	U_{22}	U_{33}	U_{12}	U_{13}	U_{23}
As1	0.0088(1)	0.0095(2)	0.0088(1)	0	0.0027(1)	0
	0.0094(1)	0.0109(2)	0.0101(1)	0	0.00359(9)	0
As2	0.0093(1)	0.0100(2)	0.0104(1)	0	0.0032(1)	0
	0.0101(1)	0.0106(2)	0.0114(1)	0	0.00416(9)	0
Fe1	0.0113(2)	0.0102(3)	0.0123(2)	0	0.0039(2)	0
	0.0115(2)	0.0101(2)	0.0131(2)	0	0.0045(1)	0
Fe2	0.0072(2)	0.0084(3)	0.0096(2)	0	0.0021(2)	0
	0.0080(2)	0.0087(2)	0.0107(2)	0	0.0031(2)	0
(Fe, Ti)	0.0174(3)	0.0159(4)	0.0116(3)	0	0.0016(2)	0
	0.0191(2)	0.0144(3)	0.0121(2)	0	0.0022(2)	0
O1	0.008(1)	0.024(2)	0.018(1)	0	0.000(1)	0
	0.0100(9)	0.022(1)	0.020(1)	0	0.0027(8)	0
O2	0.020(1)	0.023(2)	0.017(1)	0	0.010(1)	0
	0.021(1)	0.021(1)	0.0194(9)	0	0.0135(7)	0
O3	0.009(1)	0.022(2)	0.009(1)	0	0.0000(9)	0
	0.0081(8)	0.020(1)	0.0094(8)	0	0.0010(7)	0
O4	0.010(1)	0.047(3)	0.009(1)	0	0.0016(9)	0
	0.0100(9)	0.043(2)	0.0100(9)	0	0.0021(7)	0
O5	0.012(1)	0.027(2)	0.009(1)	0	0.0031(9)	0
	0.0082(8)	0.027(1)	0.0103(8)	0	0.0025(7)	0
O6	0.013(1)	0.091(5)	0.014(1)	0	0.002(1)	0
	0.010(1)	0.077(3)	0.015(1)	0	0.0034(8)	0
O7	0.023(3)	0.012(3)	0.017(2)	0	0.005(2)	0
	0.021(2)	0.015(3)	0.014(2)	0	0.005(2)	0
O8	0.033(4)	0.026(5)	0.020(3)	0	0.008(3)	0
	0.028(2)	0.024(3)	0.026(2)	0	0.014(2)	0

Note: first rows: sample A; second rows: sample B. The form of the anisotropic displacement parameter is $\exp[-2\pi^2(h^2\mathbf{a}^{*2}U_{11} + k^2\mathbf{b}^{*2}U_{22} + l^2\mathbf{c}^{*2}U_{33} + 2hk\mathbf{a}^*\mathbf{b}^*U_{12} + 2hl\mathbf{a}^*\mathbf{c}^*U_{13} + 2kl\mathbf{b}^*\mathbf{c}^*U_{23})]$ where $\mathbf{a}^*$, $\mathbf{b}^*$, and $\mathbf{c}^*$ are reciprocal lattice parameters.

TABLE 8. Selected interatomic distances (Å) and angles (°)

Sample	A	B
As1-O5	1.793(3)	1.790(2)
As1-O6	1.756(4)	1.762(3)
As1-O8[e]	1.761(3)	1.757(2)
⟨As1-O⟩	1.770	1.770
As2-O1	1.794(4)	1.792(3)
As2-O2	1.757(4)	1.754(3)
As2-O7[d]	1.746(3)	1.742(2)
⟨As2-O⟩	1.766	1.763
Fe1-O1[a]	2.142(4)	2.141(3)
Fe1-O1[b]	2.177(2)	2.173(2)
Fe1-O1[c]	2.177(2)	2.173(2)
Fe1-O3[d]	2.111(2)	2.108(2)
Fe1-O3[e]	2.111(2)	2.108(2)
Fe1-O4[g]	2.095(4)	2.093(3)
⟨Fe1-O⟩	2.136	2.133
Fe2-O2[g]	2.053(2)	2.050(2)
Fe2-O2[h]	2.053(2)	2.050(2)
Fe2-O3	1.987(3)	1.987(2)
Fe2-O5[i]	2.189(4)	2.193(2)
Fe2-O5[d]	2.160(2)	2.159(2)
Fe2-O5[e]	2.053(2)	2.050(2)
⟨Fe2-O⟩	2.083	2.082
(Ti,Fe)-O3	1.998(3)	1.991(2)
(Ti,Fe)-O4	1.976(4)	1.976(3)
(Ti,Fe)-O4[j]	2.118(2)	2.118(2)
(Ti,Fe)-O4[f]	2.118(2)	2.118(2)
(Ti,Fe)-O6[d]	2.064(3)	2.058(2)
(Ti,Fe)-O6[e]	2.064(3)	2.058(2)
⟨(Ti,Fe)-O⟩	2.056	2.053

Note: a = $x, y, 1 + z$; b = $-x, -y, 1 - z$; c = $-x, 1 - y, 1 - z$; d = $1 - x, -y, 1 - z$; e = $1 - x, 1 - y, 1 - z$; f = $2 - x, 1 - y, 1 - z$; g = $1 - x, -y, -z$; h = $1 - x, 1 - y, -z$; i = $x, y, -1 + z$; j = $2 - x, -y, 1 - z$.

state. However, such a situation is very unlikely, since in general the redox equilibrium $Fe^{3+} + Ti^{3+} \rightleftharpoons Fe^{2+} + Ti^{4+}$ is definitely shifted to the right, and no well-documented occurrence of Ti^{3+} in a terrestrial mineral has been reported.

From the above data and considerations, the theoretical composition (wt%) in terms of the constituent oxides can be deduced for both samples and is reported in Table 3. In spite of all the difficulties encountered, the agreement between the theoretical and the experimental composition is remarkable.

For the (Fe,Ti) position, the average metal to O distance (2.056 and 2.053 Å for the samples A and B, respectively) is not too different from 2.061 and 2.022 Å, the corresponding average distance for ilmenite (Ohgaki et al., 1989) and for taramellite (Mazzi and Rossi, 1980), respectively. Upon applying an empirical calculation (Brown, 1981) to the mean (Fe,Ti)-O distance, the bond-valence estimates range from 2.64 to 3.12, depending on the sample and especially on the kind of atom used as reference. Accordingly, we might reasonably assume that the average oxidation state for the atoms in this site is about +3. This implies that the oxidation state for the Fe atom in this position does not exceed +2.

The same empirical bond-valence calculation applied to the mean Fe1-O distance leads to a value of about 2.11 for the oxidation state of the metal in this site for both samples; for Fe2, the average metal to O bond length is smaller, corresponding to a bond-valence estimate of about 2.46 for both samples. In the latter case, the presence of an oxidation state intermediate between +2 and +3 is shown even more clearly. For simplicity, the oxidation state in Fe1 can be assumed to be about +2, and the state in Fe2 to be a mixture of +2 and +3.

The presence of atoms of different nature in a certain site can be verified by checking the mean-square displacement along the bond direction (Hirshfeld, 1976). Owing to the particularly rigid nature of most bonds, this displacement should be essentially the same for directly bonded atoms. Deviations in this sense are evidence for the presence of atoms differing either in nature or in the electron configuration; for ligand-metal bonds, these differences are significant if they exceed a limiting value of about 3×10^{-3} Å^2 (see for instance Bürgi, 1984; Chandrasekhar and Bürgi, 1984). Here, using data from the sample B, for either As1 or As2 the difference in mean-square displacement along each bond with the adjoining O atoms does not exceed four times the estimated standard deviation (σ). In our opinion this difference is hardly significant, since the estimated standard deviation is usually underestimated for various reasons. On the other hand, the corresponding difference for Fe1 and Fe2 amounts to 8×10^{-3} Å^2, i.e., to 7σ and to 8σ, respectively; for the (Fe,Ti) site, it is up to 35×10^{-3} Å^2, i.e., to 19σ. This essentially confirms the results obtained from the bond lengths and the occupation parameters: i.e., atoms of different kinds are located in the octahedral sites. The most reasonable assumption is that Ti replaces a

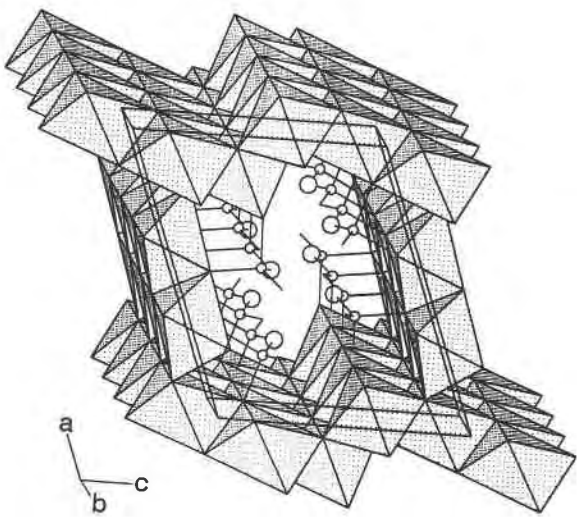

Fig. 4. Poliedri (Pilati, 1990) drawing of the structural framework seen almost along the channel direction.

substantial amount of Fe in the (Fe,Ti) site, whereas the other two metal sites are occupied essentially by Fe atoms in two oxidation states, particularly in the site Fe2.

Acknowledgments

C. Albertini has generously placed all his material from the original find at our disposal; A. Skrapits, A. Gorsatt, and R. Lüssi have provided us with the spectacular crystals from localities B and C. Preliminary chemical investigations were carried out in the SEM laboratory, Geological Institute, University of Basel (operator M. Düggelin). Help and advice from the Chairman of the Commission on New Minerals and Mineral Names, IMA, J.A. Mandarino, and of P.B. Moore is gratefully acknowledged. J.B. Saunders, from the Natural History Museum, Basel, and Suzanne Mulley have kindly corrected and commented on the English version of the manuscript.

References cited

Araki, T., Moore, P.B., and Brunton, G.D. (1980) The crystal structure of paulmooreite, $Pb_2[As_2O_5]$: Dimeric arsenite groups. American Mineralogist, 65, 340–345.

Armbruster, Th., Bühler, Ch., Graeser, S., Stalder, H.A., Amthauer, G. (1988) Cervandonite-(Ce), $(Ce,Nd,La)(Fe^{3+},Fe^{2+},Ti^{4+},Al)_3SiAs(Si,As)O_{13}$, a new Alpine fissure mineral. Schweizerische mineralogische und petrographische Mitteilungen, 68, 125–132.

Brown, I.D. (1981) The bond valence method. In M. O'Keeffe and A. Navrotsky, Eds., Structure and bonding in crystals, Academic, New York.

Bürgi, H.B. (1984) Stereochemical lability in crystalline coordination compounds. Transactions of the American Crystallographic Association, 20, 61–71.

Chandrasekhar, K., and Bürgi, H.B. (1984) Dynamic processes in crystals examined through difference vibrational parameters ΔU: The low-spin high-spin transition in tris(dithiocarbamato) iron(III) complexes. Acta Crystallographica, B40, 387–397.

Coda, A., Dal Negro, A., Sabelli, C., and Tazzoli, V. (1977) The crystal structure of stenhuggarite. Acta Crystallographica, B33, 1807–1811.

Cromer, D.T. (1974) International tables for X-ray crystallography, vol. 4, Table 2.3.1, p. 149–150. Kynoch, Birmingham, U.K.

Cromer, D.T., and Waber, J.T. (1974) International tables for X-ray crystallography, vol. 4, Table 2.2.b, p. 99–101. Kynoch, Birmingham, U.K.

Demartin, F., Gramaccioli, C.M., and Pilati, T. (1992) The importance of accurate crystal-structure determination of uranium minerals. II. The crystal structure of soddyite $(UO_2)_2(SiO_4)\cdot 2H_2O$. Acta Crystallographica, C48, 1.

Germain, G., Main, P., and Woolfson, M.M. (1971) MULTAN, a system of computer programs for the automatic solution of crystal structures from X-ray diffraction data. Acta Crystallographica, A27, 368–376.

Ghose, S., Sen Gupta, P.K., and Schlemper, E.O. (1987) Leiteite, $ZnAs_2O_4$: A novel type of tetrahedral layer structure with arsenite chains. American Mineralogist, 72, 629–632.

Graeser, S. (1966) Asbecasit und Cafarsit, zwei neue Mineralien aus dem Binntal (Kt. Wallis). Schweizerische mineralogische und petrographische Mitteilungen, 46, 367–375.

Graeser, S., and Roggiani, A.G. (1976) Occurrence and genesis of rare arsenate and phosphate minerals around Pizzo Cervandone, Italy/Switzerland. Società Italiana Mineralogia Petrografia, Rendiconti XXXII (1), 279–288.

Graeser, S., and Schwander, H. (1987) Gasparite-(Ce) and monazite-(Nd): Two new minerals to the monazite group from the Alps. Schweizerische mineralogische und petrographische Mitteilungen, 67, 103–113.

Hawthorne, F.C. (1985) Schneiderhöhnite $Fe^{2+}Fe^{3+}_3As^{3+}_5O_{13}$, a densely packed arsenite structure. Canadian Mineralogist, 23, 675–679.

Hirshfeld, F.L. (1976) Can X-ray data distinguish bonding effects from vibrational smearing? Acta Crystallographica, A32, 239–244.

Konnert, J.A., Appleman, D.E., Clark, J.R., Finger, L.W., Kato, T., and Miura, Y., (1976) Crystal structure and cation distribution of hulsite, a tin-iron borate. American Mineralogist, 61, 116–122.

Mazzi, F., and Rossi, G. (1980) The crystal structure of taramellite. American Mineralogist, 65, 123–128.

Moore, P.B., and Araki, T. (1974) Pinakiolite, $Mg_2Mn^{3+}O_2[Bo_3]$; warwickite, $Mg(Mg_{0.5}Ti_{0.5})O[BO_3]$; wightmanite, $Mg_5(O)(OH)_5[BO_3]\cdot nH_2O$: Crystal chemistry of complex 3 Å wallpaper structures. American Mineralogist, 59, 985–1004.

Ohgaki, K., Ohgaki, M., Tanaka, K., Marumo, T., and Takei, H. (1989) Electron-density distribution in ilmenite-type crystals. IV. Iron(II), titanium (IV), trioxide $FeTiO_3$. Mineralogical Journal of Japan, 14, 179–190.

Pertlik, F. (1975) Verfeinerung der Kristallstruktur von synthetischem Trippkeit, $CuAs_2O_4$. Tschermaks mineralogische und petrographische Mitteilungen, 22, 211–217.

Pilati, T. (1990) Poliedri: A Fortran program designed for plotting any kind of convex polyhedron: Communication to the XV. IUCr Congress, Bordeaux, 19–28 July 1990. Acta Crystallographica, A46, C-69.

Zemann, J. (1951) Formel und Kristallstruktur des Trippkeits. Tschermaks mineralogische und petrographische Mitteilungen, 2, 417–423.

Manuscript received August 23, 1993
Manuscript accepted May 13, 1994